





Warming-induced increase in carbon uptake is linked to earlier spring phenology in temperate and boreal forests

Hongshuang Gu^{1,4}, Yuxin Qiao^{1,4}, Zhenxiang Xi ^{1,4}, Sergio Rossi², Nicholas G. Smith ³, Jianquan Liu ¹ & Lei Chen ^{1,3}✉

Under global warming, advances in spring phenology due to rising temperatures have been widely reported. However, the physiological mechanisms underlying the advancement in spring phenology still remain poorly understood. Here, we investigated the effect of temperature during the previous growing season on spring phenology of current year based on the start of season extracted from multiple long-term and large-scale phenological datasets between 1951 and 2018. Our findings indicate that warmer temperatures during previous growing season are linked to earlier spring phenology of current year in temperate and boreal forests. Correspondingly, we observed an earlier spring phenology with the increase in photosynthesis of the previous growing season. These findings suggest that the observed warming-induced earlier spring phenology is driven by increased photosynthetic carbon assimilation in the previous growing season. Therefore, the vital role of warming-induced changes in carbon assimilation should be considered to accurately project spring phenology and carbon cycling in forest ecosystems under future climate warming.

¹Key Laboratory of Bio-Resource and Eco-Environment of Ministry of Education, College of Life Sciences, Sichuan University, Chengdu, China. ²Département des Sciences Fondamentales, Université du Québec à Chicoutimi, Chicoutimi, QC, Canada. ³Department of Biological Sciences, Texas Tech University, Lubbock, TX, USA. ⁴These authors contributed equally: Hongshuang Gu, Yuxin Qiao, Zhenxiang Xi. ✉email: lei.chen1029@gmail.com

Tree phenology influences not only the fitness and distribution of tree species, but also functioning of forest ecosystems, including water and energy fluxes and food web dynamics^{1–4}. Changes in spring phenological events (e.g., bud-break and leaf-out) that indicate the start of growing season (SOS) are highly sensitive to temperature variation, especially in the extratropical regions⁵. Under global warming, an advanced spring phenology of trees (hereafter referred to as SOS) has been widely reported over recent decades due to rising temperature^{6–8}. This advancement in SOS have been shown to extend the duration of the growing season and increase carbon uptake in forest ecosystems. Understanding the SOS in response to warming is therefore critical to assess the impacts of climate change on terrestrial carbon cycling and its feedbacks to climate^{3,9}. However, the physiological mechanisms underlying the warming-induced advancements in SOS still remain poorly understood. This largely hinders the prediction of SOS and carbon cycling under future, warmer conditions.

In temperate and boreal forests, winter and spring temperatures are traditionally considered as the primarily driver of SOS because trees need to accumulate sufficient winter chilling units to end endodormancy and spring forcing units to break ecodormancy for reactivate growth^{10–12}. Before entering dormancy, trees need to assimilate and store sufficient carbohydrates in the preceding growing season to resist the cold temperatures in winter and support growth reactivation in spring^{13–15}. In temperate and boreal trees, nonstructural carbohydrate (NSC) concentrations, such as soluble sugar and starch, often reach maximum levels in autumn before winter dormancy, but become depleted by early summer after spring growth^{16–18}. Experimental studies demonstrated that a later bud-break is often associated with a lower NSC availability in both broad-leaved and coniferous trees^{16,19–21}. The SOS of current year is therefore likely to depend on the photosynthetic carbon assimilation during the previous growing season, yet this has received little attention across large spatial and temporal scales.

Under global warming, increasing temperatures may alter photosynthetic carbon assimilation, leading to changes in tree phenology²². Photosynthetic carbon uptake tends to show a peaked response to temperature at the leaf and canopy scale^{23–26}. Collecting large-scale leaf-level photosynthesis experimental data across diverse biomes, Liang et al.²⁷ showed that climate warming increased the net photosynthetic rate by 6.13% irrespective of an increased respiration. Using FLUXNET data, Duffy et al.²⁸ demonstrated that the intersection point between photosynthesis and respiration is ~25 °C, and <10% of terrestrial biomes currently exceed this tipping point. As such, an increase in temperature during the previous growing season might increase photosynthesis in cold temperate and boreal regions, and advance SOS in the current year. However, previous studies have largely overlooked the links between previous growing season climate, photosynthesis, and the timing of SOS in the current year.

Using long-term phenological observations, digital camera imagery, remote-sensing and flux data across temperate and boreal forests in the Northern Hemisphere (Fig. 1), we analyzed the effect of warming during the previous growing season on SOS. Here we show that timing of SOS in current year is advanced by warmer temperatures during previous growing season. Furthermore, we observe that SOS of current year occurs earlier with greater photosynthetic carbon assimilation in previous growing season. Our results provide evidence that warming-induced increase in carbon assimilation could be linked to the observed earlier SOS in temperate and boreal forests under climate warming.

Results

Temperature sensitivity (S_T , change in days per degree Celsius) is expressed as the slope of a linear regression between the dates of phenological events and the temperature. This approach has been widely applied to assess phenological responses to global climate warming^{10,29,30}. To examine the effect of temperature during growing season (T_{GS}) of previous year on SOS in temperate and boreal forests, we calculated the S_T using three complementary datasets (PEP725, PhenoCam, GIMMS NDVI_{3g}). We first obtained normalized anomalies of SOS and T_{GS} at each site. Then, linear regression models were used to calculate S_T at each site separately, where the response variable was the normalized anomalies in SOS while the predictor was the normalized anomalies in T_{GS} . Negative and positive S_T indicate advanced and delayed SOS by T_{GS} , respectively.

Using the PEP725 dataset, we found that SOS was advanced by T_{GS} as indicated by the negative S_T across all selected nine temperate tree species (Fig. 2a). Among the tree species, the SOS response of *Fagus sylvatica* to T_{GS} was the strongest, and significantly higher than those of *Tilia cordata* and *Tilia platyphyllos* (Fig. 2b). To further ensure the robustness of our results, we calculated the partial correlation coefficients between T_{GS} and SOS after excluding co-variate effects of other climate variables, autumn leaf senescence, and chilling and forcing units (Supplementary Fig. 1). We observed a negative correlation between SOS and T_{GS} . This also indicated that SOS was advanced by T_{GS} .

Our PEP725 results were corroborated by PhenoCam and remote-sensing data. Specifically, we observed a negative effect of T_{GS} on SOS in deciduous broad-leaved forests and evergreen forests using phenological metrics extracted from the PhenoCam network between 2000 and 2018 (Fig. 3a). Using the phenology metrics extracted from the remote-sensing dataset between 1982 and 2014, we also observed that increasing T_{GS} advanced SOS across different vegetation types in the Northern Hemisphere (Fig. 3b). However, no significant difference in S_T among vegetation types in PhenoCam and remote-sensing datasets was detected (Fig. 3a, b).

Using the flux dataset, we found that the timing of SOS in the current year showed a significant negative correlation with the GPP_{max} , the maximum daily gross primary productivity (GPP), during previous growing season between 1992 and 2014 (Fig. 4a). We also observed a significantly negative correlation between SOS in the current year and averaged GPP in previous growing season (Supplementary Fig. 2a). This suggested that spring phenology occurred earlier when photosynthetic carbon assimilation was greater during the previous growing season. To further test the carbon-based hypothesis, we constructed a piecewise structural equation model (SEM) to explore the direct and indirect effect of climate factors on SOS (Fig. 4b and Supplementary Table 4). We found that SOS was delayed directly by temperature and soil water content, but advanced by radiation in previous season. In addition, the direct effect of CO_2 and precipitation on SOS was not significant (Fig. 4b). These direct effects are likely occurring due to spatiotemporal climate variation. We found that increased temperature and soil water content significantly increased GPP_{max} . Then, SOS was significantly advanced by increased GPP_{max} (Fig. 4b), providing evidence for indirect effects of temperature and soil water content on SOS. We obtained similar results based on the averaged GPP in previous growing season (Supplementary Fig. 2b and Supplementary Table 5). Using random-forest analysis, we calculated and ranked the relative importance of GPP_{max} and other climatic drivers to SOS. Results showed that GPP_{max} and temperature were the strongest predictors of SOS, while relative importance of precipitation, radiation, soil water content and CO_2 were lower (Fig. 5). Similar results were

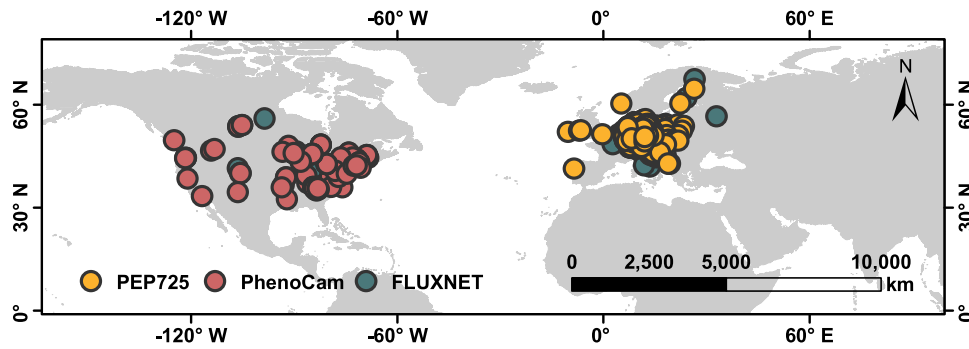


Fig. 1 Distributions of the phenological observation sites in this study. Orange dots represent the 2322 sites selected from the PEP725 dataset across central Europe. Pink and green dots represent 67 sites in North America from the PhenoCam network and 28 FLUXNET sites, respectively.

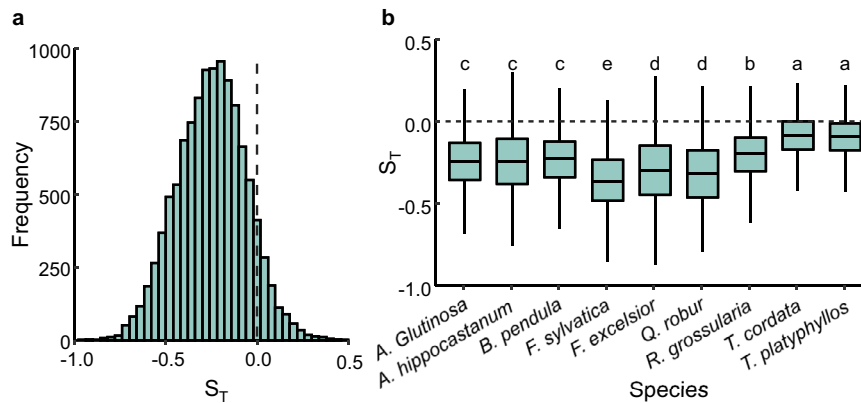


Fig. 2 Temperature sensitivities (S_T , change in days per degree Celsius) of start of season (SOS) in the current year in response to increasing temperature during previous growing season based upon PEP725 dataset. The calculated S_T was based upon records of spring leaf unfolding for 9 temperate tree species at 2322 sites in Europe. **a** Distribution of the calculated S_T across all species and sites ($N = 11,369$). **b** Difference in the S_T among tree species. The black dash lines indicate when S_T is equal to zero. The box spans from the first to the third quartile, with intermediate values marked as the black line in the middle of the box. One-way analysis of variance (ANOVA) followed by Tukey’s honestly significant difference (HSD) test was used to test the difference in the S_T between species, two-sided test was used to calculate P values and different letters indicate significant differences ($P < 0.05$). The sample size and calculated P values were listed in Supplementary Tables 2, 3.

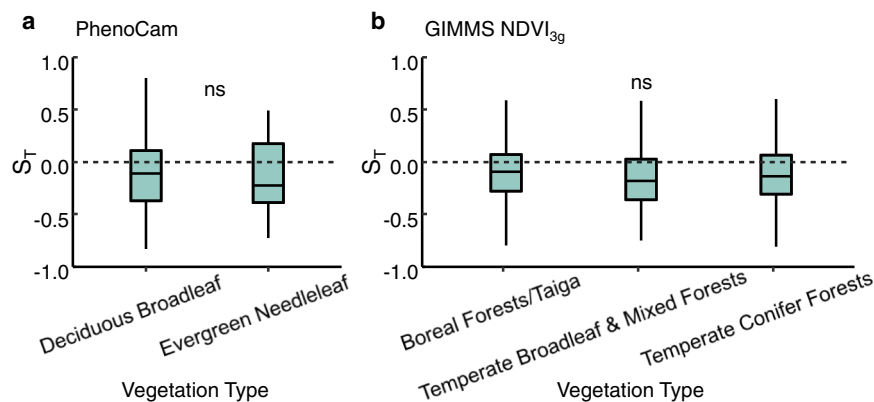


Fig. 3 Temperature sensitivities (S_T , change in days per degree Celsius) of start of season (SOS) in current year in response to increasing temperature during previous growing season. **a** The S_T based upon PhenoCam data in deciduous broadleaf and evergreen needleleaf forests. **b** The S_T based upon GIMMS NDVI_{3g} data in boreal and temperate forests. The black dash lines indicate when S_T equals zero. In the box plots, the box spans from the first to the third quartile and the median is marked as the black line. One-way analysis of variance (ANOVA) followed by Tukey’s honestly significant difference (HSD) test was used to test the differences in the S_T between vegetation types, and two-sided test was used to calculate P values, the “ns” means no significant difference between groups ($P > 0.05$). The sample size and calculated P values were listed in Supplementary Tables 2, 3.

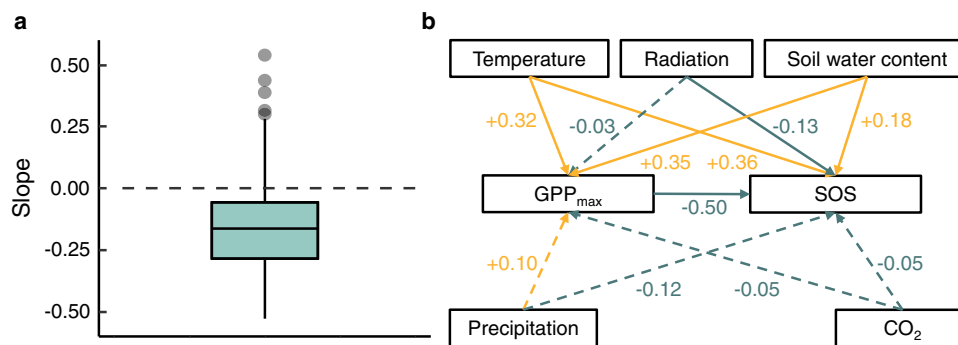


Fig. 4 Effects of GPP_{max} and climate variables on start of season (SOS) based upon FLUXNET data. **a** Regression coefficients (Slope) of normalized anomalies of SOS in current year in response to normalized anomalies of GPP_{max} in previous growing season ($N = 28$). **b** Piecewise structural equation model (SEM) considering both GPP_{max} and climate variables. The GPP_{max} refers to the maximum daily gross primary productivity (GPP) in each year. In **a**, the black dash lines indicate when slope is equal to zero, the box spans from the first to the third quartile, with intermediate values marked as the black line in the middle of the box, and the gray points represent the outliers whose values exceed 1.5 times the length of the box. In **b**, both climate factors (temperature, radiation, soil water content, precipitation, and CO_2) and GPP_{max} were incorporated into the SEM to explore the direct (arrows from each climate factor directly point to the SOS) or indirect (arrows from each climate factor firstly directly point to GPP_{max} then to the SOS) effects of climate factors on spring phenology, with green lines indicating a negative effect and orange lines indicating a positive effect. The solid lines represent significant relationships ($P < 0.05$) between variables, while dashed lines represent no significant relationships between variables ($P > 0.05$). The calculated P values based on two-sided test and other statistics were listed in Supplementary Table 4.

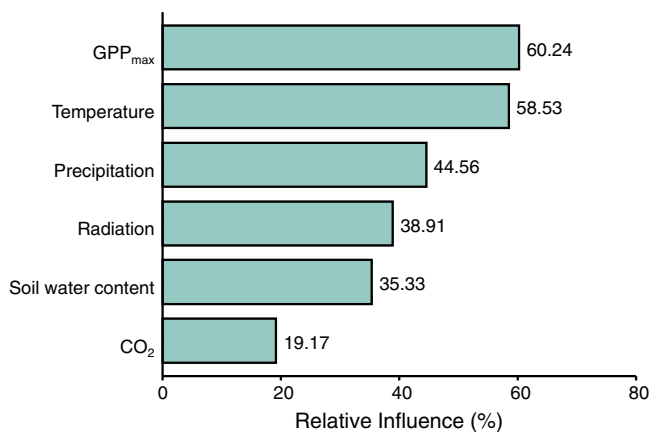


Fig. 5 Relative influence of GPP_{max} and climatic factors during previous growing season on start of season (SOS) of current year using the data of 28 FLUXNET sites between 1992 and 2014. The GPP_{max} refers to the maximum daily gross primary productivity (GPP) in each year. Random-forest algorithm was used to quantify and compare the effects of climate variables and GPP_{max} on SOS.

obtained when using averaged GPP during the previous growing season (Supplementary Fig. 3).

Discussion

Global warming has advanced bud-break and leaf-out in temperate and boreal regions^{6–8}. Using three long-term and large-scale phenological datasets, we show that warmer temperatures of the previous growing season led to earlier SOS of current year in temperate and boreal forests in the Northern Hemisphere. We also found that warming increased seasonal photosynthetic carbon assimilation, suggesting a physiological mechanism by which global warming is triggering earlier SOS in temperate and boreal forests (Fig. 6).

The carbon gained through photosynthesis can be stored in the form of nonstructural carbohydrates (NSC-soluble carbohydrates and starch), in part to support the growth of buds and leaves in the following spring^{13–15}. For instance, 95% of the starch stored in the branches of *Fagus sylvatica* and *Quercus petraea* were

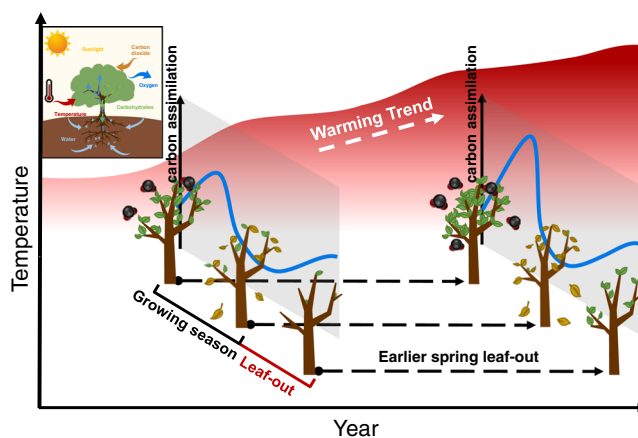


Fig. 6 A schematic diagram of the earlier spring phenology in response to warming of previous growing season. Warmer temperatures during the previous growing season drivers earlier spring phenology by increasing photosynthetic carbon assimilation.

consumed during bud break³¹. Needle growth of *Larix gmelinii* in spring drew nearly 50% of the carbohydrates fixed in the previous year^{32,33}. The starch stored in 1-year-old needles of *Picea abies* and *Pinus sylvestris* exhibited a significant decline when needle production was complete³⁴. Trees need to store sufficient carbohydrates before the winter dormancy period to maintain baseline functions and protect cells from frost damage and ensure survival in temperate and boreal regions^{35,36}. Phloem girdling experiments showed that deficient carbon storage can delay SOS in both deciduous broad-leaved and evergreen coniferous trees^{16,19}. Therefore, warmer temperatures in the previous growing season may advance SOS of current year by increasing carbon storage, supported by the negative correlations we observed between SOS of current year and GPP of previous growing season. To further test the carbon-driven hypothesis, we constructed a carbon-based SEM model to analyze the relationships between climate factors, GPP and spring phenology. We found that climate has both a direct effect on phenology, as has been shown previously^{6,37}, but also an indirect effect through

GPP. This again suggested that warming in the previous growing season may influence SOS by altering the photosynthetic carbon assimilation.

Recently, Zani et al.²² has reported that increased carbon assimilation during the growing season drives earlier autumn leaf senescence in temperate ecosystems. When leaf senescence occurred earlier, trees advanced endodormancy, and the requirement of chilling units may be also fulfilled earlier. As a result, earlier autumn phenology facilitates an earlier spring phenology^{38,39}. Therefore, increased carbon assimilation may directly drive autumn phenology, and, in turn, influence spring phenology. Furthermore, spring phenology is also influenced by chilling and forcing units in winter and spring^{29,40,41}. After excluding the co-variate effect of other climate factors in growing season, autumn phenology, chilling and forcing units on leaf unfolding, we also observed that SOS in current year was advanced by increasing temperature during the previous growing season. This provided additional support for our hypothesis that increased carbon assimilation in the previous season triggers an earlier spring phenology.

Using the PEP725 data, we observed a significant difference in the S_T among temperate tree species, which may be related to the species-specific photosynthetic leaf trait differences. For example, maximal carboxylation rate (V_{cmax}) and maximal photosynthetic electron transport rate (J_{max}) of *Quercus robur* and *Fraxinus excelsior* increased faster than *Betula pendula* with increasing temperature⁴². Correspondingly, *Quercus robur* and *Fraxinus excelsior* also showed a stronger phenological response to warming than *Betula pendula*. Using PhenoCam and remote-sensing data, we compared the difference in the S_T between deciduous broad-leaved and evergreen conifer forests, but no significant difference was observed between them. Compared with evergreens, the leaf life-span is shorter in deciduous species, and thus the time window allowed for photosynthesis is shorter^{43,44}. However, deciduous species usually hold a larger leaf size and higher photosynthetic capacity than evergreens^{45,46}. This could compensate for their shorter leaf life-span, and may partly explain the observed similar phenological responses between deciduous and evergreen forests.

Despite the warming-induced spring phenology observed in temperate and boreal regions, the underlying causes and physiological mechanisms still remain unclear. Using multiple long-term and large-scale datasets, herein we demonstrated that an increase in carbon assimilation under global warming could be involved in the observed earlier spring phenology in temperate and boreal forests. Our study provides new insights into the warming-induced change in spring phenology under global climate change to predict spring phenology and vegetation-atmosphere feedbacks under future climatic scenarios.

Methods

PEP725 phenological network. Phenological observation data were acquired by the European phenology database PEP725 (<http://www.pep725.eu/>). PEP725 contains phenological observations of temperate species across central Europe starting in 1951⁴⁷. We selected the date when the first leaf stalks were visible (BBCH11 in PEP725) to represent SOS and date when 50% leaves had their autumnal color (BBCH94 in PEP725) to represent the end of growing season (EOS). Data exceeding 2.5 times of median absolute deviation (MAD) were considered outliers and removed⁴⁸. We selected 466,988 records of nine temperate tree species (Supplementary Table 1) at 2322 sites, for a total of 171,202 species-site combinations with at least 30 years of observations.

PhenoCam network. The PhenoCam network (<https://phenocam.sr.unh.edu/>) is a cooperative database of digital camera imagery that provides the dates of phenological transition between 2000 and 2018 across a diverse vegetations in Northern America⁴⁹. In the PhenoCam network, the 50%, 75% and 90% of the Green Chromatic Coordinate (G_{CC}) were calculated daily to extract the date of greenness

rising and falling based on the following formula:

$$G_{CC} = \frac{G_{DN}}{R_{DN} + G_{DN} + B_{DN}}, \quad (1)$$

where R_{DN} , G_{DN} , and B_{DN} are the average red, green and blue digital numbers (DN), respectively.

We selected 50% amplitude of G_{CC-90} (G_{CC} reaches 90th quantiles of its seasonal amplitude) as SOS⁵⁰. We removed outliers when exceeding 2.5 times of MAD, and selected sites with at least 8-year observations between 2000 and 2018. Because we restricted study area to temperate and boreal forests, we excluded non-forest sites in the PhenoCam dataset. The final dataset had a total of 67 sites across deciduous broadleaf and evergreen coniferous forests.

GIMMS NDVI_{3g} phenological product. The Normalized Difference Vegetation Index (NDVI), a proxy of vegetation greenness and photosynthetic activity, is commonly used to derive phenological metrics⁵¹. We derived SOS from the third generation GIMMS NDVI_{3g} dataset (<http://ecocast.arc.nasa.gov>) from Advanced Very High Resolution Radiometer (AVHRR) instruments for the period 1982–2014 with a spatial resolution of 8 km and a temporal resolution of 15 days⁵².

We only kept areas outside tropics (latitudes >30°N) that have a clear seasonal phenology⁵³ and excluded bare lands with annual average NDVI < 0.1 to reduce bias. We applied a Savitzky-Golay filter⁵⁴ to smooth the time series and eliminate noise of atmospheric interference and satellite sensor, and used a Double Logistic 1st order equation to extract phenology dates⁵³ according to the formula:

$$y(t) = a \left(\frac{1}{1 + e^{k(t-m)}} + \frac{1}{1 + e^{n(t-n)}} \right) + b, \quad (2)$$

where a , k , m , and n are parameters of logistic function and a is the initial background NDVI value, $a + b$ represents the maximum NDVI value, t is time in days, and $y(t)$ is the NDVI value at time t . The second-order derivative of Eq. 2 was calculated to extract SOS and EOS at the first and second local maximum point, respectively^{55,56}. We excluded tropical and subtropical forests, and non-forest vegetation types based on a map of terrestrial ecoregions and focused on northern temperate and boreal forests⁵⁷. The selected forest biomes include Boreal Forests/Taiga, Temperate Conifer Forests, and Temperate Broadleaf and Mixed Forests.

FLUXNET dataset. The flux dataset was downloaded from FLUXNET (<https://fluxnet.org/data/>). The FLUXNET-2015 dataset was released in November 2016 (Total: 212 sites worldwide)⁵⁸. The FLUXNET-2015 dataset provides data at different time scales, including half-hourly, daily, weekly, and yearly. The data at daily, weekly, and yearly scales were generated based on the original half-hour data using a data processing pipeline⁵⁸, which was applied to reduce uncertainty by improving the data quality control and generate uniform and high-quality derived data products suitable for studies that compare multiple sites⁵⁸. To be consistent with the temporal resolution of PEP725 and PhenoCam data, we selected daily-scale data from the FLUXNET-2015 dataset. Because we focused on temperate and boreal forests in the Northern Hemisphere, we selected a total of 28 forest sites with at least 10-years of observations and >300 daily records per year between 1992 and 2014 in the Northern Hemisphere. Here, we used mean GPP and GPP_{max} (the maximum daily GPP) during previous growing season to evaluate the photosynthetic carbon fixation at the ecosystem scale^{59–61}. Singular Spectrum Analysis (SSA) filter method was first used to smooth the time series of daily GPP to minimize the noise^{62,63}. The annual GPP_{max} was then obtained by extracting the maximum daily GPP values in each year from the smoothed GPP curve. The average GPP was calculated as the mean daily GPP during growing season between May and September. The SOS was extracted from smoothed daily GPP curve based on the threshold method⁵⁴. The spring threshold was defined as 15% of the multi-year daily GPP maximum following previous studies^{64,65}, and SOS was defined as the turning point when the smoothed GPP was higher than spring threshold.

Climate data. Gridded daily mean temperature (°C), solar radiation (Wm^{-2}), air humidity (%) and daily total precipitation (mm) during 1950–2015 in Europe were downloaded from the database E-OBS (<http://www.ecad.eu/>)⁶⁶ at 0.25° spatial resolution. Gridded monthly soil moistures (kg/m^2) during 1979–2015 were downloaded from World Meteorological Organization (http://climexp.knmi.nl/select.cgi?id=someone@somewhere&field=clm_wfdei_soil01) at 0.5° spatial resolution and banded with PEP725 dataset. Global monthly mean temperatures during 1981–2017 were downloaded from Climate Research Unit (https://crudata.uea.ac.uk/cru/data/hrg/cru_ts_4.04/; <http://www.geodata.cn>) at 0.5° spatial resolution to match the PhenoCam and GIMMS NDVI_{3g} datasets. Bilinear interpolation method was used to extract climate data of each site or pixel using the “raster” package⁶⁷ in R⁶⁸. Environmental variables, including daily mean temperature (°C), shortwave radiation (Wm^{-2}), CO₂ (ppm), and precipitation (mm) were also extracted from the FLUXNET dataset. The detailed information of all the datasets used in our study was listed in Supplementary Table 6.

Statistical analyses. The phenological records from PEP725 network are direct observations in the field, have a higher quality, and cover a longer period (1951–2015). However, most sites of PEP725 network are located in Central Europe and constrained

to a relatively small spatial scale. In contrast, the extracted phenological metrics from PhenoCam images and remote-sensing products cover a large spatial scale regardless of their shorter periods. Therefore, we combined them together when performing statistical analyses to ensure precision and representativeness of our results.

We first calculated the temperature sensitivity (S_T , change in days per degree Celsius) based on mean temperatures during the previous growing season (T_{GS}) and timing of SOS using the three complementary datasets (PEP725, PhenoCam, GIMMS NDMI_{3g}) in the Northern Hemisphere. The S_T was defined as the slope of linear regression between the dates of phenological stages and the temperature^{10,29,30}. The mean dates of SOS and EOS from the PEP725 network were DOY 120 and DOY 280. Therefore, the period between May and September was selected to represent the growing season. A similar time period was used for complimentary analyses of PhenoCam and GIMMS NDMI_{3g} data. To calculate the S_T , we first obtained normalized anomalies of SOS and T_{GS} relative to their long-term average at each site or pixel. Then, linear regression models were used to calculate S_T at each site or pixel separately, in which the response variable was the normalized anomalies in SOS while the predictor was the normalized anomalies in T_{GS} . One-way analysis of variance (ANOVA) followed by Tukey's honestly significant difference (HSD) test was used to test the difference in the S_T between species and vegetation types.

In addition to temperature, other climate factors (e.g., radiation and precipitation) may influence SOS by altering leaf photosynthesis. Partial correlation analysis has been frequently used to exclude confounding effects in order to isolate the relationship between two variables⁶⁹. Using partial correlation analysis, here we excluded potential co-variate effects of a set of climate variables of growing season, including radiation, precipitation, soil moisture, humidity, on SOS and further examined the relationship between T_{GS} and SOS in PEP725 network. Because radiation and soil moisture data were only available since 1980, we selected phenology and climate datasets between 1984 and 2015.

Commonly, temperatures in winter and spring act as the dominant driver of spring phenology by influencing the accumulation of chilling and forcing units^{29,37}. Importantly, effect of autumn phenology on spring phenology has been also reported^{38,39}. To ensure the robustness of results, therefore, we also calculated the partial correlation coefficient between T_{GS} and SOS after excluding the co-variate effects of EOS and accumulations of chilling and forcing units, respectively, to test the relationship between T_{GS} and SOS in PEP725 network. Accumulations of chilling and forcing units were calculated during the period between November 1st and mean SOS across years for each species at each site¹⁰. The chilling units were calculated as the number of chilling days when daily mean temperature ranged from 0 to 5 °C; and the forcing units were calculated as the accumulated growing degree days when the daily mean temperature was above the threshold temperature 5 °C^{10,70}. We performed partial correlation analysis using "ppcor" package⁷¹ in R⁶⁸.

To clarify the underlying physiological mechanisms, we further examined the relationships between GPP (both average GPP and GPP_{max}) of the previous growing season and SOS between 1992 and 2014 using FLUXNET data. Because the site-averaged daily GPP from FLUXNET started to increase from DOY 120, peaking at DOY 180, then decreased until DOY 300, the period between May and September was also selected as the growing season for calculating the climate variables. This is also consistent with the period of growing season identified by the dates of leaf unfolding and leaf senescence in PEP725 network. To examine the relationship between SOS and average GPP_{max}, we first obtained normalized anomalies of SOS and GPP_{max} relative to their long-term average at each site. Then, linear regression models were applied to analyze the relationship between GPP_{max} anomalies on SOS anomalies for each site separately. In the models, the response variable was the normalized anomalies in SOS of current year and the predictor was normalized anomalies in GPP_{max} of previous growing season. The 95% confidence interval of the site-level regression slopes was calculated to determine the statistical significance of the relationship between GPP anomalies and SOS anomalies. The same analysis was repeated for average GPP instead of GPP_{max}.

We further used piecewise structural equation models (SEM) to analyze the relationships between climate, GPP (both average GPP and GPP_{max}) and SOS from the FLUXNET sites⁷². To test our carbon-based hypothesis, we constructed a conceptual model that includes both the direct and indirect effects of climate factors in growing season on spring phenology. In the SEM model, we hypothesized that climate during the growing season is likely to directly influence the timing of spring phenology, i.e., plants can directly sense the change in climate factors and determine the onset of spring phenology, indicated by the arrows from each climate factor directly point to the SOS. Also, they can indirectly influence spring phenology by altering the photosynthetic carbon assimilation, indicated by the arrows from each climate factor firstly directly point to GPP or GPP_{max} then to the SOS. The piecewise SEM was fit using the "piecewiseSEM" package⁷² in R⁶⁸.

Further, we quantified and compared effects of these climate variables and GPP_{max} on spring phenology using random-forest algorithm, an ensemble statistical learning method⁷³ that has been frequently applied in ecological modeling and prediction^{74,75}. By this, we select the most important variables which may affect forest phenology, including GPP_{max}, temperature, precipitation, radiation, CO₂, and soil water content in FLUXNET between 1992 and 2014. We conducted random forests analysis using "randomForest" package⁷⁶ in R⁶⁸, where the number of trees (ntree) and variables randomly sampled as candidates (mtry) at each split were set to 1000 and 4 respectively to guarantee the reliability of the result⁷⁷. These same analyses were repeated using average GPP in place of GPP_{max}. All data analyses were conducted using R version 4.0.3⁶⁸.

Reporting summary. Further information on research design is available in the Nature Research Reporting Summary linked to this article.

Data availability

The PEP725 phenological data was accessed from www.pep725.eu, PhenoCam phenological data was obtained from <https://phenocam.sr.unh.edu/>, GIMMS NDMI_{3g} dataset was downloaded from <http://ecocast.arc.nasa.gov>, FLUXNET dataset was downloaded from <https://fluxnet.org/data/>. Climate data were downloaded from E-OBS (<http://ensembles-eu.metoffice.com>), World Meteorological Organization (http://climexp.knmi.nl/select.cgi?id=someone@somewhere&field=clm_wfdei_soil01) and Climate Research Unit (https://crudata.uea.ac.uk/cru/data/hrg/cru_ts_4.04/; <http://www.geodata.cn>).

Code availability

The primary codes used in this study are available at https://figshare.com/articles/software/code_information/20037647.

Received: 23 February 2022; Accepted: 21 June 2022;

Published online: 27 June 2022

References

1. Chuine, I. Why does phenology drive species distribution? *Philos. Trans.* **365**, 3149–3160 (2010).
2. Chuine, I. & Beaubien, E. G. Phenology is a major determinant of tree species range. *Ecol. Lett.* **4**, 500–510 (2001).
3. Richardson, D. A. et al. Climate change, phenology, and phenological control of vegetation feedbacks to the climate system. *Agric. For. Meteorol.* **169**, 156–173 (2013).
4. Tang, J. et al. Emerging opportunities and challenges in phenology: a review. *Ecosphere* **7**, e01436 (2016).
5. Piao, S. et al. Plant phenology and global climate change: current progresses and challenges. *Glob. Chang. Biol.* **25**, 1922–1940 (2019).
6. Fu, Y. H. et al. Three times greater weight of daytime than of night-time temperature on leaf unfolding phenology in temperate trees. *N. Phytol.* **212**, 590–597 (2016).
7. Menzel, A. et al. European phenological response to climate change matches the warming pattern. *Glob. Chang. Biol.* **12**, 1969–1976 (2006).
8. Piao, S. et al. Leaf onset in the northern hemisphere triggered by daytime temperature. *Nat. Commun.* **6**, 6911 (2015).
9. Penuelas, J., Rutishauser, T. & Filella, I. Phenology feedbacks on climate change. *Science* **324**, 887–888 (2009).
10. Fu, Y. H. et al. Declining global warming effects on the phenology of spring leaf unfolding. *Nature* **526**, 104–107 (2015).
11. Lang, G. A. Dormancy: a new universal terminology. *HortScience* **22**, 817–820 (1987).
12. Perry, T. O. Dormancy of trees in winter. *Science* **171**, 29–36 (1971).
13. Huang, J. et al. Intra-annual wood formation of subtropical Chinese red pine shows better growth in dry season than wet season. *Tree Physiol.* **38**, 1225–1236 (2018).
14. Knowles, J. F. et al. Montane forest productivity across a semi-arid climatic gradient. *Glob. Chang. Biol.* **26**, 6945–6958 (2020).
15. Richard, S., Kjellens, T. D., Schaberg, P. G. & Murakami, P. F. Dynamics of low-temperature acclimation in temperate and boreal conifer foliage in a mild winter climate. *Tree Physiol.* **28**, 1365–1374 (2008).
16. Roxas, A. A., Orozco, J., Guzmán-Delgado, P. & Zwieniecki, M. A. Spring phenology is affected by fall non-structural carbohydrate concentration and winter sugar redistribution in three Mediterranean nut tree species. *Tree Physiol.* **41**, 1425–1438 (2021).
17. Palacio, S., Martínez, M. M. & Montserrat-Martí, G. Seasonal dynamics of non-structural carbohydrates in two species of mediterranean sub-shrubs with different leaf phenology. *Environ. Exp. Bot.* **59**, 34–42 (2007).
18. Fierravanti, A., Rossi, S., Kneeshaw, D., Grandpré, L. D. & Deslauriers, A. Low non-structural carbon accumulation in spring reduces growth and increases mortality in conifers defoliated by spruce budworm. *Front. For. Glob. Change.* **2**, 1–13 (2019).
19. Oberhuber, W., Gruber, A., Lethaus, G., Winkler, A. & Wieser, G. Stem girdling indicates prioritized carbon allocation to the root system at the expense of radial stem growth in Norway spruce under drought conditions. *Environ. Exp. Bot.* **138**, 109–118 (2017).
20. Pérez-de-Lis, G., Rossi, S., Vázquez-Ruiz, R. A., Rozas, V. & García-González, I. Do changes in spring phenology affect earlywood vessels? Perspective from the xylogenesis monitoring of two sympatric ring-porous oaks. *N. Phytol.* **209**, 521–530 (2016).

21. Weber, R., Gessler, A. & Hoch, G. High carbon storage in carbon-limited trees. *N. Phytol.* **222**, 171–182 (2019).
22. Zani, D., Crowther, T. W., Lidong, M., Renner, S. S. & Zohner, C. M. Increased growing-season productivity drives earlier autumn leaf senescence in temperate trees. *Science* **370**, 1066–1071 (2020).
23. Dusenke, M. E., Duarte, A. G. & Way, D. A. Plant carbon metabolism and climate change: elevated CO₂ and temperature impacts on photosynthesis, photorespiration and respiration. *N. Phytol.* **221**, 32–49 (2019).
24. Lin, Y.-S., Medlyn, B. E. & Ellsworth, D. Temperature responses of leaf net photosynthesis: the role of component processes. *Tree Physiol.* **32**, 219–231 (2012).
25. Huang, M. et al. Air temperature optima of vegetation productivity across global biomes. *Nat. Ecol. Evol.* **3**, 772–779 (2019).
26. Terashima, I. & Hikosaka, K. Comparative ecophysiology of leaf and canopy photosynthesis. *Plant Cell Environ.* **18**, 1111–1128 (1995).
27. Liang, J., Xia, J., Liu, L. & Wan, S. Global patterns of the responses of leaf-level photosynthesis and respiration in terrestrial plants to experimental warming. *J. Plant. Ecol.* **6**, 437–447 (2013).
28. Duffy, K. A. et al. How close are we to the temperature tipping point of the terrestrial biosphere? *Sci. Adv.* **7**, eaay1052 (2021).
29. Güsewell, S., Furrer, R., Gehrig, R. & Pietragalla, B. Changes in temperature sensitivity of spring phenology with recent climate warming in Switzerland are related to shifts of the pre-season. *Glob. Chang. Biol.* **23**, 5189–5202 (2017).
30. Keenan, T. F., Richardson, A. D. & Hufkens, K. On quantifying the apparent temperature sensitivity of plant phenology. *N. Phytol.* **225**, 1033–1040 (2020).
31. Klein, T., Vitasse, Y. & Hoch, G. Coordination between growth, phenology and carbon storage in three coexisting deciduous tree species in a temperate forest. *Tree Physiol.* **36**, 847–855 (2016).
32. Kagawa, A., Sugimoto, A. & Maximov, T. C. Seasonal course of translocation, storage and remobilization of ¹³C pulse-labeled photoassimilate in naturally growing *Larix gmelinii* saplings. *N. Phytol.* **171**, 793–804 (2010).
33. Rinne, K. T. et al. Examining the response of needle carbohydrates from Siberian larch trees to climate using compound-specific δ(13) C and concentration analyses. *Plant Cell Environ.* **38**, 2340–2352 (2015).
34. Schädel, C., Blöchl, A., Richter, A. & Hoch, G. Short-term dynamics of nonstructural carbohydrates and hemicelluloses in young branches of temperate forest trees during bud break. *Tree Physiol.* **29**, 901–911 (2009).
35. Kaurin, A., Junttila, O. & Hanson, J. Seasonal changes in frost hardiness in cloudberry (*Rubus chamaemorus*) in relation to carbohydrate content with special reference to sucrose. *Physiol. Plant.* **52**, 310–314 (1981).
36. Shahba, M. A., Qian, Y. L., Hughes, H. G., Koski, A. J. & Christensen, D. Relationships of soluble carbohydrates and freeze tolerance in saltgrass. *Crop Sci.* **43**, 2148–2153 (2003).
37. Wang, J. et al. Contrasting temporal variations in responses of leaf unfolding to daytime and nighttime warming. *Glob. Chang. Biol.* **27**, 5084–5093 (2021).
38. Marchand, L. J. et al. Inter-individual variability in spring phenology of temperate deciduous trees depends on species, tree size and previous year autumn phenology. *Agric Meteorol.* **290**, 108031 (2020).
39. Shen, M. et al. Can changes in autumn phenology facilitate earlier green-up date of northern vegetation? *Agric Meteorol.* **291**, 108077 (2020).
40. Chen, L. et al. Long-term changes in the impacts of global warming on leaf phenology of four temperate tree species. *Glob. Chang. Biol.* **25**, 997–1004 (2019).
41. Hanninen, H. Boreal and temperate trees in a changing climate: modelling the ecophysiology of seasonality. (Springer, 2016).
42. Dreyer, E., Le Roux, X., Montpied, P., Daudet, F. A. & Masson, F. Temperature response of leaf photosynthetic capacity in seedlings from seven temperate tree species. *Tree Physiol.* **21**, 223–232 (2001).
43. Devi, A. F. & Garkoti, S. C. Variation in evergreen and deciduous species leaf phenology in Assam. *India Trees* **27**, 985–997 (2013).
44. Bai, K., He, C., Wan, X. & Jiang, D. Leaf economics of evergreen and deciduous tree species along an elevational gradient in a subtropical mountain. *AoB PLANTS* **7**, plv064 (2015).
45. Qi, J., Fan, Z., Fu, P., Zhang, Y. & Sterck, F. Differential determinants of growth rates in subtropical evergreen and deciduous juvenile trees: carbon gain, hydraulics and nutrient-use efficiencies. *Tree Physiol.* **41**, 12–23 (2021).
46. Fyllas, N. M. et al. Functional trait variation among and within species and plant functional types in mountainous mediterranean forests. *Front. Plant Sci.* **11**, 1–18 (2020).
47. Templ, B. et al. Pan European Phenological database (PEP725): a single point of access for European data. *Int J. Biometeorol.* **62**, 1109–1113 (2018).
48. Leys, C., Ley, C., Klein, O., Bernard, P. & Licata, L. Detecting outliers: do not use standard deviation around the mean, use absolute deviation around the median. *J. Exp. Soc. Psychol.* **49**, 764–766 (2013).
49. Richardson, A. D. et al. Tracking vegetation phenology across diverse North American biomes using PhenoCam imagery. *Sci. Data.* **5**, 180028 (2018).
50. Klosterman, S. et al. Evaluating remote sensing of deciduous forest phenology at multiple spatial scales using PhenoCam imagery. *Biogeosciences* **11**, 4305–4320 (2014).
51. Zhang, Y. et al. Seasonal and interannual changes in vegetation activity of tropical forests in Southeast Asia. *Agric. For. Meteorol.* **224**, 1–10 (2016).
52. Pinzon, J. E. & Tucker, C. J. A non-stationary 1981–2012 AVHRR NDVI3g time series. *Remote Sens.* **6**, 6929–6960 (2014).
53. Wang, X. et al. No trends in spring and autumn phenology during the global warming hiatus. *Nat. Commun.* **10**, 2389 (2019).
54. Wang, X. et al. Validation of MODIS-GPP product at 10 flux sites in northern China. *Int. J. Remote Sens.* **34**, 587–599 (2013).
55. Julien, Y. & Sobrino, J. Global land surface phenology trends from GIMMS database. *Int. J. Remote Sens.* **30**, 3495–3513 (2009).
56. Zhang, X. et al. Monitoring vegetation phenology using MODIS. *Remote Sens Environ.* **84**, 471–475 (2003).
57. Dinerstein, E. et al. An ecoregion-based approach to protecting half the terrestrial realm. *Bioscience* **67**, 534–545 (2017).
58. Pastorello, G. et al. The FLUXNET2015 dataset and the ONEFlux processing pipeline for eddy covariance data. *Sci. Data.* **7**, 1–27 (2020).
59. Huang, K. et al. Enhanced peak growth of global vegetation and its key mechanisms. *Nat. Ecol. Evol.* **2**, 1897–1905 (2018).
60. Tang, Y., Xu, X., Zhou, Z., Qu, Y. & Sun, Y. Estimating global maximum gross primary productivity of vegetation based on the combination of MODIS greenness and temperature data. *Ecol. Inform.* **63**, 101307 (2021).
61. Xia, J. et al. Joint control of terrestrial gross primary productivity by plant phenology and physiology. *Proc. Natl. Acad. Sci. U.S.A.* **112**, 2788–2793 (2015).
62. Kalman, D. A singularly valuable decomposition: The SVD of a matrix. *Coll. Math. J.* **27**, 2–23 (1996).
63. Biriukova, K. et al. Performance of singular spectrum analysis in separating seasonal and fast physiological dynamics of solar-induced chlorophyll fluorescence and PRI optical signals. *J. Geophys. Res. Biogeosci.* **126**, e2020JG006158 (2021).
64. Richardson, A. D. et al. Influence of spring and autumn phenological transitions on forest ecosystem productivity. *Philos. Trans. R. Soc. Lond. B Biol. Sci.* **365**, 3227–3246 (2010).
65. Wu, C. et al. Interannual variability of net carbon exchange is related to the lag between the end-dates of net carbon uptake and photosynthesis: Evidence from long records at two contrasting forest stands. *Agric. For. Meteorol.* **164**, 29–38 (2012).
66. Cornes, R., der Schrier, G. V., den Besselaar, E. J. M. V. & Jones, P. An ensemble version of the E-OBS temperature and precipitation data sets. *J. Geophys. Res. Atmos.* **123**, 9391–9409 (2018).
67. Hijmans, R. J. et al. raster: Geographic data analysis and modeling. <https://CRAN.R-project.org/package=raster>. R package version 3.5-15 (2022).
68. R Core Team. R: A language and environment for statistical computing. R Foundation for Statistical Computing, Vienna, Austria (2021).
69. Erb, I. Partial correlations in compositional data analysis. *Comput. Geosci.* **6**, 100026 (2020).
70. Vitasse, Y., Signarbieux, C. & Fu, Y. H. Global warming leads to more uniform spring phenology across elevations. *Proc. Natl. Acad. Sci. U.S.A.* **115**, 1004–1008 (2018).
71. Kim, S. ppcor: Partial and semi-partial (part) correlation. <https://CRAN.R-project.org/package=ppcor>. R package version 1.1 (2015).
72. Lefcheck, J. S. piecewiseSEM: piecewise structural equation modeling in R for ecology, evolution, and systematics. *Methods Ecol. Evol.* **7**, 573–579 (2016).
73. Breiman, L. Random forests. *Mach. Learn.* **45**, 5–32 (2001).
74. Valavi, R., Elith, J., Lahoz-Monfort, J. J. & Guillera-Arroita, G. Modelling species presence-only data with random forests. *Ecography* **44**, 1731–1742 (2021).
75. Freeman, E. A., Moisen, G. G., Coulston, J. W. & Wilson, B. T. Random forests and stochastic gradient boosting for predicting tree canopy cover: comparing tuning processes and model performance. *Can. J. For. Res.* **46**, 323–339 (2016).
76. Liaw, A. & Wiener, M. Classification and regression by randomForest. *R. N.* **2**, 18–22 (2002).
77. Cutler, D. et al. Random forests for classification in ecology. *Ecology* **88**, 2783–2792 (2007).

Acknowledgements

We acknowledge all members of the PEP725 network for collecting and providing the phenological data. This research was funded by National Natural Science Foundation of China (31590821 and 91731301). N.G.S. and L.C. acknowledge support from Texas Tech University.

Author contributions

L.C. designed the research. H.G. and Y.Q. performed the data analysis. Y.Q. and H.G. wrote the paper with the inputs of L.C., S.R., N.G.S., and J.L.. All authors contributed to the interpretation of the results and approved the final paper.

Competing interests

The authors declare no competing interests.

Additional information

Supplementary information The online version contains supplementary material available at <https://doi.org/10.1038/s41467-022-31496-w>.

Correspondence and requests for materials should be addressed to Lei Chen.

Peer review information *Nature Communications* thanks Eric Beamesderfer and the other, anonymous, reviewer(s) for their contribution to the peer review of this work.

Reprints and permission information is available at <http://www.nature.com/reprints>

Publisher's note Springer Nature remains neutral with regard to jurisdictional claims in published maps and institutional affiliations.



Open Access This article is licensed under a Creative Commons Attribution 4.0 International License, which permits use, sharing, adaptation, distribution and reproduction in any medium or format, as long as you give appropriate credit to the original author(s) and the source, provide a link to the Creative Commons license, and indicate if changes were made. The images or other third party material in this article are included in the article's Creative Commons license, unless indicated otherwise in a credit line to the material. If material is not included in the article's Creative Commons license and your intended use is not permitted by statutory regulation or exceeds the permitted use, you will need to obtain permission directly from the copyright holder. To view a copy of this license, visit <http://creativecommons.org/licenses/by/4.0/>.

© The Author(s) 2022, corrected publication 2022